

# Measurement of extreme-ultraviolet attenuation edges of magnesium, tin, and indium filters

John Seely and Benjawan Kjornrattanawanich

We determined the energies of the Mg  $L_{2,3}$ , Sn  $N_{4,5}$ , and In  $N_{4,5}$  attenuation edges by measuring the transmission of high-resolution synchrotron radiation through thin filters. The Al  $L_{2,3}$  and Si  $L_3$  edges observed in the first and higher diffraction orders from the monochromator were used as energy fiducials. For each attenuation edge, the onset of attenuation with increasing energy and the inflection point of the attenuation curve were measured. The measured energy values were compared with previously determined attenuation edge energies and with electron binding energies. The measured energies of the inflection points are Mg  $L_2$  ( $49.89 \pm 0.02$  eV), Mg  $L_3$  ( $49.58 \pm 0.02$  eV), Sn  $N_4$  ( $25.00 \pm 0.02$  eV), Sn  $N_5$  ( $23.97 \pm 0.02$  eV), In  $N_4$  ( $17.66 \pm 0.02$  eV), and In  $N_5$  ( $16.70 \pm 0.02$  eV). © 2003 Optical Society of America

OCIS codes: 310.6860, 350.2450.

## 1. Introduction

Transmission filters composed of thin metal films are commonly utilized in the extreme-ultraviolet region.<sup>1</sup> When used as part of a spectrometer or monochromator that disperses radiation from a broadband source, the filter's useful range extends from the wavelength of an attenuation edge to nearly twice that wavelength, above which shorter wavelengths (e.g., from higher diffraction orders of a grating) can in some circumstances pass through the filter and contaminate the spectral bandpass of interest. In general, the filter is utilized to establish a wavelength bandpass, attenuate shorter wavelengths that might contaminate the bandpass of interest, block longer wavelengths and visible light, and provide protection at an instrument's entrance aperture from thermal loading. In addition, the filter's attenuation edges observed in the first and higher diffraction orders can serve as convenient wavelength references, and this application of attenuation edge wavelengths is the primary motivation for the present study.

Aluminum has been one of the most extensively studied filter materials for wavelengths longer than the Al  $L_{2,3}$  attenuation edge near 17 nm, culminating with the development of the unbacked and robust aluminum filters for the solar instruments on the Skylab space station.<sup>2</sup> Other useful filters included tin and indium for wavelengths longer than their  $N_{4,5}$  attenuation edges near 50 and 74 nm, respectively.<sup>3,4</sup>

The wavelengths of the  $L$  attenuation edges of aluminum and silicon filters have been accurately measured.<sup>5-7</sup> The wavelength of a filter's  $L$  attenuation edge is related to the binding energy of the  $2p$  electrons in the solid material.<sup>8,9</sup> However, the energy of the attenuation edge and the nearby structure depend on the binding energy of the core level and the energy distribution of the unoccupied states in the solid, the conduction band just above the Fermi level in the case of a metal such as aluminum and the conduction band in the case of crystalline silicon. The unoccupied states can vary in an amorphous material and can be altered by molecular and surface effects. When a filter edge is used as a wavelength reference, it is therefore necessary to accurately measure the edge wavelength of the filter that is actually utilized and not rely on tabulated binding energies.

In this work, the wavelengths of Mg  $L_{2,3}$  filter edges were accurately measured by use of the previously determined Al  $L_{2,3}$  and Si  $L_3$  filter edges as wavelength references. Then, with the higher-order Al  $L_{2,3}$  and Mg  $L_{2,3}$  filter edges used as wavelength references, the wavelengths of the Sn  $N_{4,5}$  and In  $N_{4,5}$  edges were measured. The measured edge wave-

---

J. Seely (john.seely@nrl.navy.mil) is with the Space Science Division, Code 7674, U.S. Naval Research Laboratory, 4555 Overlook Avenue, SW, Washington, D.C. 20375. B. Kjornrattanawanich is with the Universities Space Research Association, National Synchrotron Light Source, Beamline X24C, Brookhaven National Laboratory, Upton, New York 11973.

Received 25 April 2003; revised manuscript received 16 July 2003.

0003-6935/03/316374-08\$15.00/0

© 2003 Optical Society of America

lengths are compared with previous values and selected electron binding energies.

This study extends the accurate measurement of filter edges from Si  $L_3$  (12.434 nm, 99.716 eV), Al  $L_2$  (16.949 nm, 73.153 eV), and Al  $L_3$  (17.050 nm, 72.718 eV) to longer wavelengths: Mg  $L_2$  (24.851 nm, 49.892 eV), Mg  $L_3$  (25.005 nm, 49.584 eV), Sn  $N_4$  (49.59 nm, 25.00 eV), Sn  $N_5$  (51.74 nm, 23.97 eV), In  $N_4$  (70.20 nm, 17.66 eV), and In  $N_5$  (74.24 nm, 16.70 eV). These reference wavelengths should be useful to establish the wavelength scales of spectrometers and monochromators utilized for the observation of laboratory, solar, astrophysical, and synchrotron radiation sources in the extreme-ultraviolet region.

## 2. Experimental Technique

The filter edges were observed with the beamline X24C at the National Synchrotron Light Source at Brookhaven National Laboratory.<sup>10–12</sup> The radiation from the storage ring was dispersed by a monochromator composed of a gold mirror and a 600-groove/mm diffraction grating with a 2° blaze angle. The mirror and grating were accurately translated and rotated under computer control. The two types of motion, on-blaze and off-blaze, are illustrated in Fig. 1. An on-blaze motion consisted of translating and rotating the mirror and grating so that a desired wavelength propagated through the fixed monochromator exit slit while equalizing the angles of incidence and diffraction on the grating groove facets (the on-blaze condition). An off-blaze wavelength scan was performed by first moving the mirror and grating to the desired on-blaze wavelength positions and then rotating the grating, without otherwise moving the grating and mirror, and thereby varying the wavelength that propagated through the fixed exit slit.

The procedure that was used to measure the filter transmittances was to move the monochromator grating and mirror in the on-blaze manner to a wavelength near the filter edges to be observed, sequentially position the selected filters in the dispersed beam, and for each filter to scan the wavelength in the off-blaze manner while the transmitted radiation was recorded with a silicon photodiode. Thus the accuracy of the measurements primarily depended on the accuracy and reproducibility of the grating rotational motion.

The monochromator grating was rotated in the following manner. A motor located outside the monochromator vacuum chamber rotated a precision lead screw that translated a rod that was rigidly connected by a metal band to the perimeter of a wheel located inside the vacuum chamber. The grating was mounted on a carousel at the center of rotation of the wheel. Thus the translational motion of the rod was directly coupled to the rotational motion of the grating. The translational motion was measured by an encoder with a precision of  $\pm 0.5 \mu\text{m}$ . The computer control system iterated on the translational position until the  $\pm 0.5\text{-}\mu\text{m}$  precision was achieved as indicated by the feedback from the encoder. The radius of the wheel was 17.78 cm, and the  $\pm 0.5\text{-}\mu\text{m}$

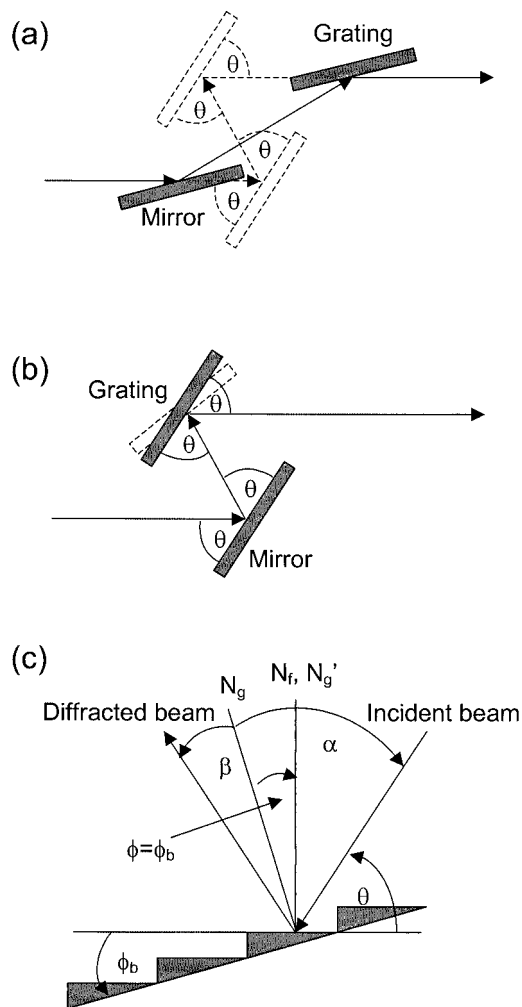


Fig. 1. Monochromator motions in (a) the on-blaze condition where the mirror and the grating are both translated and rotated to make equal grazing angles on the mirror and on the grating groove facets and (b) the off-blaze condition where only the grating is rotated after the desired on-blaze angle is set. (c) Shown is the grating geometry in an on-blaze condition ( $\phi = \phi_b$ ).  $N_g$  and  $N_f$  are the normals to the grating and to the groove facets, respectively.  $N_g'$  is the normal to the grating when the grating is rotated off blaze to a diffracted angle  $\beta$  that is equal to an incident angle  $\alpha$  and of opposite sign (zero-order diffraction condition). The monochromator exit slit fixes the output direction, and only wavelengths that satisfy the grating equation can pass through it.

precision in the translational motion corresponded to a  $\pm 2.8\text{-}\mu\text{rad}$  precision in the grating rotation angle.

The wavelength that propagated through the exit slit and was incident on the selected filter was determined by the grating equation

$$m\lambda = d(\sin \alpha + \sin \beta), \quad (1)$$

where  $m$  is the diffraction order ( $m > 0$  for inside orders,  $m < 0$  for outside orders);  $d$  is the groove spacing; and  $\alpha$  and  $\beta$  are the angle of incidence and the angle of diffraction measured from the grating normal, respectively. The angle  $\beta$  is negative if it falls on the opposite side of the grating normal from  $\alpha$ . Because the direction of the input beam that

strikes the gold mirror and the direction of the output beam that diffracts through the exit slit of the monochromator are fixed, Eq. (1) reduces to a more convenient form<sup>10</sup>:

$$m\lambda = 2d \sin \phi \sin \theta, \quad (2)$$

where  $\theta$  is the on-blaze grazing angle and  $\phi$  is the angular rotation of the grating normal relative to its position at zero-order diffraction as illustrated in Fig. 1(c). The angle  $\phi$  is equal to the blaze angle ( $\phi_b$ ) for the on-blaze condition and is zero for the case of zero-order diffraction through the exit slit. Note that Eq. (2) has the form of the Bragg equation for on-blaze operation where  $d \sin \phi_b$ , the height of the triangular groove, is analogous to the crystal lattice spacing.<sup>13</sup> Thus for on-blaze wavelength scans the radiation diffracted from the groove facets constructively interferes in the same manner as diffraction from a crystal lattice.

The monochromator computer control system was designed to propagate the first inside order through the exit slit. However, the grating equation is also satisfied for wavelengths in higher orders, when  $|m| > 1$ . Hence for a fixed angle of incidence, the shorter wavelengths ( $\lambda/m$ ) have the same diffraction angle as the first-order radiation and can also propagate through the exit slit. When the filter's transmission spectrum is plotted with respect to the first-order wavelengths, the attenuation edges under some circumstances can be observed in the first-order wavelength region and also at multiples of the first-order wavelengths in the higher-order radiation. Such an observation of attenuation edges in various orders is a means of transferring the wavelength calibration scale to longer wavelengths and is a standard practice in extreme-ultraviolet spectroscopy.

In general, the higher-order observations are facilitated when off-blaze wavelength scans are performed in a manner in which the grating has relatively large efficiency in the higher orders.<sup>10</sup> Since during an off-blaze wavelength scan only one motor rotates the grating, the motion is simple, more precise, and reproducible compared with an on-blaze wavelength scan, where all four motors are used to translate and rotate the grating and mirror. Therefore the filter transmittances were measured with off-blaze wavelength scans used to accurately determine the attenuation edge wavelengths of a number of filters in their first and higher orders.

### 3. Magnesium, Aluminum, and Silicon Attenuation Edges

A 264-nm-thick magnesium filter, 300-nm aluminum filter, and 500-nm silicon filter were utilized. The magnesium filter, as fabricated by the Luxel Corporation by evaporation, had a 32.2-nm aluminum capping layer on each side of the 264-nm magnesium layer for the purpose of protecting the magnesium from oxidation. Previous studies of this filter indicated that, although the aluminum layers had sur-

face oxidation, there was no evidence of oxidation of the interior magnesium layer.<sup>14</sup>

In observations of the magnesium, aluminum, and silicon attenuation edges, the monochromator was first moved to an on-blaze grazing angle  $\theta$  of 12.83° (on-blaze wavelength of 25.8 nm). Each filter was sequentially positioned in the dispersed beam, and the wavelength was then scanned in the off-blaze manner by varying  $\phi$  in Eq. (2) while keeping  $\theta$  fixed. The radiation transmitted by each filter was recorded with a silicon photodiode detector.

For measurements at an on-blaze grazing angle  $\theta$  of 12.83°, the  $\pm 2.8$ - $\mu$ rad precision in the grating rotation angle corresponded to a  $\pm 2 \times 10^{-5}$ -nm precision in the first-order wavelength that was propagated through the center of the monochromator exit slit. The spread in wavelength through a 100- $\mu$ m-wide slit, located a distance of 12.5 m from the grating, was  $4 \times 10^{-3}$  nm. The radiation beam size, approximately 2 mm,<sup>15</sup> and aberration effects reduced the resolving power to approximately 600, which at the on-blaze wavelength of 25.8 nm corresponds to a wavelength resolution of 0.04 nm. This is smaller than the expected splitting of the  $L_2$  and  $L_3$  edge features of magnesium (0.14 nm),<sup>16</sup> aluminum (0.10 nm),<sup>17</sup> and silicon (0.08 nm).<sup>18</sup>

The photodiode signal resulting from the transmission of radiation through the magnesium filter was normalized to zero at wavelengths shorter than the Mg  $L_{2,3}$  edges and to unity at longer wavelengths. The resulting values were subtracted from unity and are a representation of the attenuation curve. The magnesium filter attenuation curve is plotted as a function of the energy of the radiation that was incident on the filter in Fig. 2(a). Energy is plotted rather than wavelength to facilitate comparison with previously published electron binding energies and attenuation edge energies. The conversion factor 1239.852 eV/nm was utilized. The first and second derivatives of the observed magnesium filter attenuation curve are shown in Figs. 2(b) and 2(c), respectively. The maxima of the first derivative represent the inflection points of the  $L_2$  and  $L_3$  attenuation features. The onsets of the  $L_2$  and  $L_3$  attenuation features are determined from the maxima of the second derivative. Similar attenuation curves were recorded for the aluminum and silicon filters by the same off-blaze scanning technique. Calculations indicated that the energies of the inflection points were insensitive to the thickness of the filter over the range of thicknesses that were studied.

Using the transmission spectrum, we initially based the attenuation edge energies on the energy scale that was derived from the geometry of the monochromator. We then more accurately determined the energy scale by comparing the initially measured attenuation edges with the reference aluminum and silicon filter edge energies of previous researchers.

The reference energies for the aluminum inflection points were from Codling and Madden.<sup>5</sup> They measured the attenuation edges of aluminum filters us-

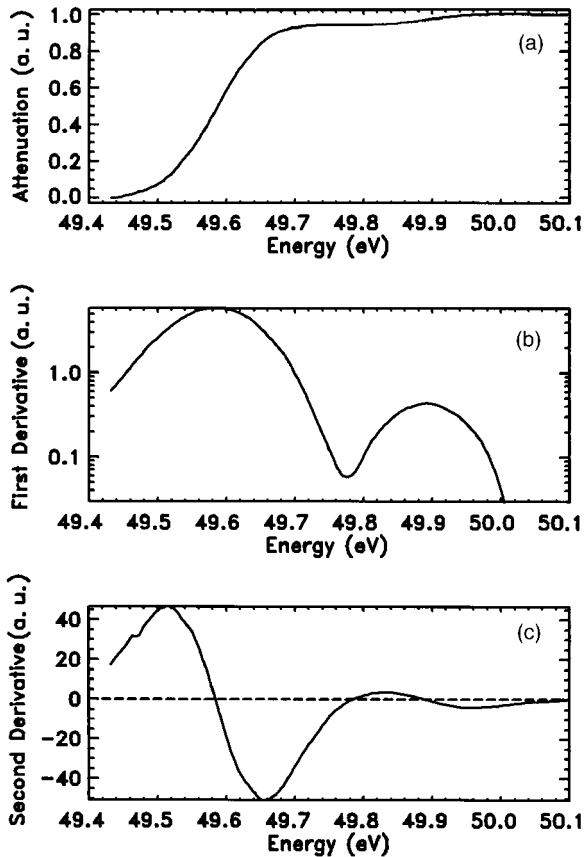


Fig. 2. (a) Observed magnesium filter attenuation curve, (b) the first derivative of the magnesium filter attenuation curve, (c) the second derivative of the magnesium filter attenuation curve.

ing synchrotron radiation and a 3-m grazing-incidence spectrometer. The aluminum filters were prepared by evaporation, were approximately 100 nm thick, and were mounted on nickel fine-mesh screens. The wavelength calibration was established to an accuracy of 0.002 nm by He II reference lines. The wavelengths were measured at the points of maximum slopes (the inflection points) of the attenuation curves. The measured wavelengths of the Al  $L_2$  and  $L_3$  attenuation edges were 16.949 and 17.049 nm, respectively, with an uncertainty of  $\pm 0.005$  nm. Therefore the reference energies are 73.152 and 72.723 eV with uncertainties  $\pm 0.02$  eV.

The wavelength of the Si  $L_3$  attenuation edge of a silicon filter was accurately measured by Gullikson *et al.*<sup>6,7</sup> using synchrotron radiation. The measured value was 12.434 nm with an uncertainty of  $\pm 0.002$  nm. The corresponding edge energy is  $99.715 \pm 0.016$  eV.

The silicon  $L$  attenuation edges were also observed by Brown and Rustgi<sup>19</sup> using synchrotron radiation. They observed the  $L$  attenuation edges of amorphous and crystalline silicon films with thicknesses in the 100–200-nm range. The Si  $L_3$  edge energy, measured at the inflection point of the attenuation curve, was  $99.84 \pm 0.06$  eV. This energy is 0.125 eV larger than the value from Refs. 6 and 7,  $99.715 \pm 0.016$  eV,

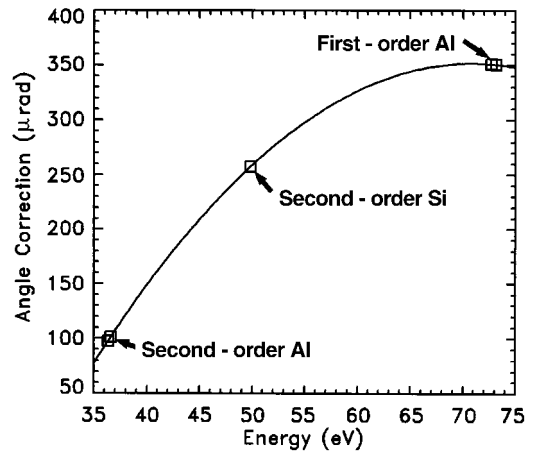


Fig. 3. Correction to the grating rotation angle that is based on the reference energies of the aluminum and silicon attenuation edges.

and the difference exceeds the uncertainties. Comparisons of the Si  $L_3$  edge energy from Ref. 19 with the aluminum edges presently observed in the first and higher orders indicate that the value from Ref. 19 is inconsistent with the aluminum reference energies of Ref. 5. Therefore the Si  $L_3$  edge energy of Refs. 6 and 7,  $99.715 \pm 0.016$  eV, is adopted as the reference energy.

Although the energies of the attenuation edges that were initially measured, by use of the energy scale from the monochromator geometry, were remarkably precise and reproducible, the absolute values had large systematic differences from the reference energies. These differences resulted from the inaccuracy of the on-blaze grating rotation angle  $\theta$  and from possible nonlinearities in the grating rotation encoder scale. The value of  $12.83^\circ$  was based on the geometry of the monochromator and the energy scale established prior to this study by filter edge energies that were measured with a wider exit slit (600  $\mu\text{m}$ ) with lower spectral resolution. Therefore a systematic correction was applied to the grating rotation angle based on the reference energies of the aluminum and silicon filter edges.

The energy correction that was applied to the off-blaze scans through the filters was determined in the following manner. For each energy scan through a particular filter, the energies of the attenuation edges were first calculated by use of the grating equation and the fixed on-blaze grating angle  $\theta = 12.83^\circ$ , the initial value of the grating rotation angle  $\phi$ , and the values of the change in  $\phi$  that were precisely measured by the encoded grating rotational motion. Then, by use of the aluminum and silicon reference energies, the corrected values of the rotation angle  $\phi$  were calculated. As shown in Fig. 3, it was found that the corrections to the values of the grating rotation angle at the Al  $L_{2,3}$  filter edges observed in the first and second orders and the Si  $L_3$  filter edge observed in the second order varied with the edge energy over the range 96–349  $\mu\text{rad}$ , much larger than

Table 1. Mg, Al, and Si Attenuation Edge Energies

Designation	Order	Edge	Present (eV)	Previous (eV)	Difference (eV)
Al $L_2$	1	Onset	73.072		
	1	Inflection	73.153	$73.152 \pm 0.02^a$	0.001
Al $L_3$	1	Onset	72.640		
	1	Inflection	72.718	$72.723 \pm 0.02^a$	-0.005
Mg $L_2$	1	Onset	49.836		
	1	Inflection	49.892		
Si $L_3$	2	Onset	49.745		
	2	Inflection	49.858	$49.857 \pm 0.008^b$	0.001
Mg $L_3$	1	Onset	49.512		
	1	Inflection	49.584		
Al $L_2$	2	Onset	36.545		
	2	Inflection	36.580	$36.576 \pm 0.01^a$	0.004
Al $L_3$	2	Onset	36.303		
	2	Inflection	36.362	$36.361 \pm 0.01^a$	0.001

<sup>a</sup>Reference 5.

<sup>b</sup>References 6 and 7.

the 2.8- $\mu$ rad precision of the grating rotation angle. With the least-squares technique, a quadratic polynomial was fitted to the five values of the correction angles, weighted by the inverse of the uncertainties in the reference values. Then the energies of the aluminum, silicon, and magnesium edges were recalculated with this correction curve.

The measured energy values derived from the observed attenuation curves of the magnesium, aluminum, and silicon filters are listed in the fourth column of Table 1. Listed are the onset and inflection energies of the Mg  $L_2$  and  $L_3$  features observed in the first diffraction order, the Al  $L_2$  and  $L_3$  features observed in the first and second orders, and the Si  $L_3$  feature observed in the second order. The aluminum energies fall on each side of the magnesium energies, and the silicon energy is quite close to the Mg  $L_2$  and  $L_3$  energies. Thus the corrected energy scale used to measure the Mg  $L_2$  and  $L_3$  energies is well determined by the aluminum and silicon reference energies.

In Table 1 the aluminum and silicon reference energies are listed in the fifth column with their uncertainties. The differences between the reference energies and the presently determined energies, based on the correction curve for the grating rotation angle, are listed in the last column and are plotted in Fig. 4(a). The differences between the five previously determined aluminum and silicon inflection energies and the present measurements are 0.005 eV or less.

Considering the high precision of the present measurements and the excellent consistency with the previously measured silicon and aluminum reference energies (with uncertainties of  $\pm 0.02$  eV or less), the accuracy of the presently determined Mg  $L_2$  and  $L_3$  filter attenuation inflection points is estimated to be  $\pm 0.02$  eV. Thus the presently determined Mg  $L_2$  and  $L_3$  filter attenuation inflection energies are  $49.892 \pm 0.02$  and  $49.584 \pm 0.02$  eV, respectively. The latter value is consistent with the Mg  $L_3$  attenuation edge reported by Hagemann *et al.*,<sup>20</sup>  $49.5 \pm 0.3$  eV.

#### 4. Sn and In Attenuation Edges

The attenuation edges of a 110-nm-thick tin filter and a 110-nm indium filter were observed. The energy scans were performed at grating on-blaze angles of 18.00° or 33.37°. These values are larger than the

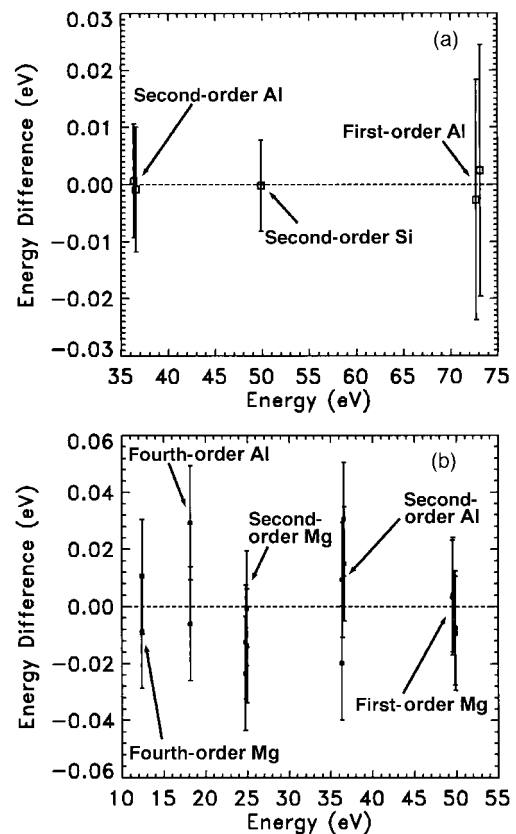


Fig. 4. Differences between the presently determined and the previously determined (a) magnesium, aluminum, and silicon attenuation edge energies observed in the first and second orders and (b) magnesium and aluminum attenuation edge energies observed up to the fourth order.

Table 2. Mg, Al, Sn, and In Attenuation Edge Energies

Designation	Order	Edge	Present (eV)	Previous <sup>a</sup> (eV)	Difference (eV)
Mg $L_2$	1	Onset	49.828	49.836 ± 0.02	-0.008
	1	Inflection	49.882	49.892 ± 0.02	-0.010
Mg $L_3$	1	Onset	49.515	49.512 ± 0.02	0.003
	1	Inflection	49.588	49.584 ± 0.02	0.004
Al $L_2$	2	Onset	36.567	36.536 ± 0.02	0.031
	2	Inflection	36.591	36.576 ± 0.02	0.015
Al $L_3$	2	Onset	36.300	36.320 ± 0.02	-0.020
	2	Inflection	36.368	36.359 ± 0.02	0.009
Sn $N_4$	1	Onset	24.922		
	1	Inflection	25.002		
Mg $L_2$	2	Onset	24.917	24.918 ± 0.02	-0.001
	2	Inflection	24.932	24.946 ± 0.02	-0.014
Mg $L_3$	2	Onset	24.732	24.756 ± 0.02	-0.024
	2	Inflection	24.780	24.792 ± 0.02	-0.012
Sn $N_5$	1	Onset	23.753		
	1	Inflection	23.965		
Al $L_3$	4	Onset	18.154	18.160 ± 0.02	-0.006
	4	Inflection	18.209	18.180 ± 0.02	0.029
In $N_4$	1	Onset	17.545		
	1	Inflection	17.663		
In $N_5$	1	Onset	16.605		
	1	Inflection	16.701		
Mg $L_3$	4	Onset	12.369	12.378 ± 0.02	-0.009
	4	Inflection	12.406	12.396 ± 0.02	0.010

<sup>a</sup>Table 1, column 4.

on-blaze angle of 12.83° that was used to observe the low-order magnesium, aluminum, and silicon edges because the tin and indium attenuation edges occur at lower energies. Because of the lower signal levels for the scans in this energy region, the monochromator exit slit was widened to 200 or 400 μm from the 100-μm slit width used for the low-order magnesium, aluminum, and silicon edges. Although the wider slit resulted in larger energy spread, the spectral resolution was sufficient to observe the tin and indium  $N_4$  and  $N_5$  features.

The energies of the Sn  $N_{4,5}$  and In  $N_{4,5}$  edges were measured by use of the aluminum and magnesium edges observed in the higher orders as energy references. The aluminum and magnesium filter scans were performed in the same manner as the tin and indium filter scans, with the same on-blaze grating angle and slit width. The aluminum edges were observed in the second and fourth orders, and the magnesium edges were observed in the first, second, and fourth orders. The values of the higher-order aluminum and magnesium  $L_{2,3}$  energies that were used as references were derived from the first-order values in Table 1, column 4. As discussed at the end of Section 3, the uncertainty of these aluminum and silicon edge energies are estimated to be 0.02 eV. The energy scale was established through fitting a quadratic polynomial to the 16 aluminum and magnesium reference energies, and the tin and indium energies were measured with respect to this energy scale. The differences between the fitted edge energies and the reference energies derived from Table 1 are listed in the last column in Table 2. The standard deviation of the energy difference values is 0.015

eV and is within the estimated 0.02-eV uncertainty in the aluminum and silicon energy references.

As can be seen in Table 2, the magnesium and aluminum reference energies spanned the tin and indium edge energies and served as excellent energy references. The measured tin and indium edge energies are listed in the fourth column in Table 2, and the estimated accuracy of these values is ±0.02 eV, the same as the accuracy of the aluminum and silicon energy references from Table 1, column 4.

The Sn  $N_{4,5}$  attenuation edges were observed by Codling *et al.*<sup>3</sup> in the transmission spectra of tin filters with thicknesses in the range 68–169 nm. The edge energies, measured at the points of maximum slope, were 24.9 ± 0.1 and 23.8 ± 0.1 eV for the Sn  $N_4$  and  $N_5$  features, respectively. These values are lower than the presently measured values of 25.00 ± 0.02 and 23.97 ± 0.02 eV, and in the case of Sn  $N_5$  the value of Codling *et al.*<sup>3</sup> is beyond the uncertainties.

The unresolved tin and indium  $N$  attenuation features were observed in the transmission spectra of a 102-nm-thick tin filter and an 80-nm-thick indium filter by Walker *et al.*<sup>21</sup> The values of the Sn  $N$  and In  $N$  edges were 24.3 and 16.8 eV, respectively. These values fall in the range of the presently determined energies listed in Table 2 for Sn  $N_{4,5}$  (23.75–25.00 eV) and In  $N_{4,5}$  (16.61–17.66 eV). Hunter *et al.*<sup>4</sup> also observed the unresolved indium  $N$  attenuation feature in the transmission spectrum of an 80-nm-thick filter, and the measured In  $N$  edge energy was 17.0 eV.

Jezequel *et al.*<sup>22</sup> inferred the attenuation coefficients of tin and indium from reflectance measurements using synchrotron radiation. The spectral

**Table 3. Electron Binding Energies and Presently Measured Inflection Points of the Filter Attenuation Curves**

Designation	Binding Energy (eV)	Present Energy <sup>a</sup> (eV)	Present Wavelength (nm)
Si $L_3$	$99.8 \pm 0.1^b$	$99.716 \pm 0.02$	$12.434 \pm 0.002$
Al $L_2$	$73.1 \pm 0.1^b$	$73.153 \pm 0.02$	$16.949 \pm 0.005$
Al $L_3$	$72.7 \pm 0.1^b$	$72.718 \pm 0.02$	$17.050 \pm 0.005$
Mg $L_2$	$49.9 \pm 0.1^b$	$49.892 \pm 0.02$	$24.851 \pm 0.01$
Mg $L_3$	$49.5 \pm 0.1^b$	$49.584 \pm 0.02$	$25.005 \pm 0.01$
Sn $N_4$	$25.00 \pm 0.15^c$	$25.00 \pm 0.02$	$49.59 \pm 0.04$
Sn $N_5$	$23.95 \pm 0.12^c$	$23.97 \pm 0.02$	$51.74 \pm 0.04$
In $N_4$	$17.66 \pm 0.15^c$	$17.66 \pm 0.02$	$70.20 \pm 0.08$
In $N_5$	$16.80 \pm 0.12^c$	$16.70 \pm 0.02$	$74.24 \pm 0.08$

<sup>a</sup>Tables 1 and 2.

<sup>b</sup>Reference 23.

<sup>c</sup>Reference 24.

resolution was sufficient to resolve the  $N_4$  and  $N_5$  features. The energies of the points of maximum slope were determined with an uncertainty of 0.05 eV. The Sn  $N_4$  and  $N_5$  values were 24.88 and 23.75 eV and the In  $N_4$  and  $N_5$  values were 17.65 and 16.72 eV, respectively. The tin values are significantly lower than the presently determined values, and the indium values are in good agreement with the present values. It should be noted that the attenuation coefficients determined indirectly from reflectance measurements are quite sensitive to the surface conditions of the sample, whereas attenuation coefficients determined directly from filter transmittance measurements are more characteristic of the bulk material.

### 5. Comparison with Binding Energies

The filter attenuation edge energies are related to the electron binding energies determined by x-ray photoelectron spectroscopy and other techniques. The  $L_2$  and  $L_3$  attenuation edge energies are related to the  $2p_{1/2}$  and  $2p_{3/2}$  binding energies and the  $N_4$  and  $N_5$  attenuation energies to the  $4d_{3/2}$  and  $4d_{5/2}$  binding energies, respectively. Primarily because of uncertainties in the work function, uncertainties in the tabulated binding energies are typically in the 0.1–0.2-eV range, much larger than the uncertainties (0.02 eV) in the measurements of the filter attenuation edge energies.

Listed in Table 3 are the presently measured energies of the inflection points of the filter attenuation curves and the corresponding electron binding energies from Refs. 23 and 24. The values are in agreement within the rather large uncertainties in the binding energies. Thus, in general, the tabulated binding energies represent approximate values for the filter attenuation edge energies, but the direct measurement of the edge energies by use of high-resolution synchrotron radiation results in more accurate values.

### 6. Conclusion

High-resolution synchrotron radiation was used to accurately measure the attenuation edges of magnesium, aluminum, silicon, tin, and indium filters in the first and higher diffraction orders from the monochro-

mator. The previously measured aluminum and silicon edges were used as energy references. The measured edge energies, with an estimated uncertainty of 0.02 eV, were consistent with the electron binding energies within the relatively large uncertainties (0.10–0.15 eV) in the binding energy values. The presently measured filter edge energies should serve as accurate energy fiducials in the extreme-ultraviolet region. The energies and the corresponding wavelengths of the inflection points of the filter attenuation curves are listed in the last two columns of Table 3.

This research was supported by grants from the National Aeronautics and Space Administration and the U.S. Office of Naval Research. The National Synchrotron Light Source is supported by the U.S. Department of Energy. We thank Jack Rife and William Hunter for beneficial discussions concerning the operation of the monochromator.

### References

1. J. A. R. Samson, *Techniques of Vacuum Ultraviolet Spectroscopy* (Pied Publications, Lincoln, Neb., 1967).
2. R. J. Schumacher and W. R. Hunter, "Thin aluminum filters for use on the Apollo Telescope Mount XUV spectrographs," *Appl. Opt.* **16**, 904–908 (1977).
3. K. Codling, R. P. Madden, W. R. Hunter, and D. W. Angel, "Transmittance of tin films in the far ultraviolet," *J. Opt. Soc. Am.* **56**, 189–192 (1966).
4. W. R. Hunter, D. W. Angel, and R. Tousey, "Thin films and their uses for the extreme ultraviolet," *Appl. Opt.* **4**, 891–898 (1965).
5. K. Codling and R. P. Madden, "Structure in the  $L_{II,III}$  absorption of aluminum and its oxides," *Phys. Rev.* **167**, 587–591 (1968).
6. E. M. Gullikson, P. Denham, S. Mrowka, and J. H. Underwood, "Absolute photoabsorption measurements of Mg, Al, and Si in the soft x-ray region," *Phys. Rev. B* **49**, 16283–16286 (1994).
7. E. M. Gullikson, Center for X-Ray Optics, Lawrence Berkeley National Laboratory, Berkeley, Calif. (personal communication, 2002).
8. R. D. Deslattes and E. G. Kessler, "Experimental evaluation of inner-vacancy level energies for comparison with theory," in *Atomic Inner-Shell Physics*, B. Crasemann, ed. (Plenum, New York, 1985).
9. K. Siegbahn, C. Nordling, A. Fahlman, R. Nordberg, K. Hamrin, J. Hedman, G. Johansson, T. Bergmark, S.-E. Karls-

- son, I. Lindgren, and B. Lindberg, *ESCA Atomic, Molecular and Solid State Structure Studied by Means of Electron Spectroscopy* (Almqvist and Wiksells Boktryckeri AB, Uppsala, Sweden, 1967).
10. W. R. Hunter and J. C. Rife, "Higher-order suppression in an on-blaze plane-grating monochromator," *Appl. Opt.* **23**, 293–299 (1984).
  11. J. C. Rife, W. R. Hunter, and R. T. Williams, "Features and initial performance tests of the grating/crystal monochromator," *Nucl. Instrum. Methods Phys. Res. A* **246**, 252–255 (1986).
  12. J. C. Rife, H. R. Sadeghi, and W. R. Hunter, "Upgrades and recent performance of the grating/crystal monochromator," *Rev. Sci. Instrum.* **60**, 2064–2067 (1989).
  13. J. C. Rife, W. R. Hunter, T. W. Barbee, and R. G. Cruddace, "Multilayer-coated blazed grating performance in the soft x-ray region," *Appl. Opt.* **28**, 2984–2986 (1989).
  14. J. F. Seely, "Extreme-ultraviolet thin-film interference in an Al-Mg-Al multiple-layer transmission filter," *Appl. Opt.* **41**, 5979–5983 (2002).
  15. J. F. Seely, C. M. Brown, G. E. Holland, F. Hanser, J. Wise, J. L. Weaver, R. Korde, R. A. Viereck, R. Grubb, and D. L. Judge, "Calibration of an extreme-ultraviolet transmission grating spectrometer with synchrotron radiation," *Appl. Opt.* **40**, 1623–1630 (2001).
  16. P. M. Th. M. Van Attekum and J. M. Trooster, "The resolution obtainable in x-ray photoelectron spectroscopy with unmonochromatized Mg K $\alpha$  radiation," *J. Electron. Spectrosc. Relat. Phenom.* **18**, 135–143 (1980).
  17. S. B. M. Hagström, R. Z. Bachrach, and R. S. Bauer, "Oxidation of aluminum surfaces studied by synchrotron radiation photoelectron spectroscopy," *Phys. Ser.* **16**, 414–419 (1977).
  18. J. C. Woicik, T. Kendelewicz, K. Miyano, R. Cao, P. Pianetta, I. Lindau, and W. E. Spicer, "Semiconductor surface core level shifts by use of selected overlayers," *Phys. Scr.* **41**, 1034–1036 (1990).
  19. F. C. Brown and O. P. Rustgi, "Extreme ultraviolet transmission of crystalline and amorphous silicon," *Phys. Rev. Lett.* **28**, 497–500 (1972).
  20. H.-J. Hagemann, W. Gudat, and C. Kunz, "Optical constants from the far infrared to the x-ray region: Mg, Al, Cu, Ag, Bi, C, and Al<sub>2</sub>O<sub>3</sub>," DESY SR-74/7 (Deutsches Elektronen-Synchrotron DESY, Hamburg, Germany, 1974).
  21. W. C. Walker, O. P. Rustgi, and G. L. Weissler, "Optical and photoelectric properties of thin metallic films in the vacuum ultraviolet," *J. Opt. Soc. Am.* **49**, 471–475 (1959).
  22. G. Jezequel, J. Thomas, and J. C. Lemonnier, "Optical transitions from d core states in polycrystalline indium, tin, and lead," *Solid State Commun.* **23**, 559–562 (1977).
  23. Center for X-Ray Optics, Lawrence Berkeley National Laboratory, Berkeley, Calif., [www-cxro.lbl.gov](http://www-cxro.lbl.gov) (2002).
  24. R. Nyholm and N. Martensson, "Core level binding energies for the elements Zr-Te (Z = 40-52)," *J. Phys. C* **13**, L279–L284 (1980).